Conf-910624--3

TITLE OF SYMPOSIUM OR TITLE OF ASTM JOURNAL:

23rd National Symposium on Fracture Mechanics

CONF-910624--3

DE91 013410

AUTHOR'S NAME:

David K.M. Shum[1] and John G. Merkle[1]

TITLE OF PAPER:

Crack Initiation Under Generalized Plane Strain Conditions*

AUTHOR'S AFFILIATIONS

[1]Research specialists, Oak Ridge National Laboratory, Oak Ridge, TN 37831

---

*Research sponsored by the Office of Nuclear Regulatory Research, U.S. Nuclear Regulatory Commission under Interagency Agreement 1886-8011-9B with the U.S. Department of Energy under Contract DE-AC05-84OR21400 with Martin Marietta Energy Systems, Inc.

Re: Manuscript for the 23rd National Symposium

Authors: David K.M. Shum and John G. Merkle
Title: Crack Initiation Under Generalized Plane Strain Conditions

ABSTRACT: A method for estimating the decrease in crack-initiation toughness, from a reference plane strain value, due to positive straining along the crack front of a circumferential flaw in a reactor pressure vessel is presented in this study. This method relates crack initiation under generalized plane strain conditions with material failure at points within a distance of a few crack-tip-opening displacements ahead of a crack front, and involves the formulation of a micromechanical crack-initiation model. While this study is intended to address concerns regarding the effects of positive out-of-plane straining on ductile crack initiation, the approach adopted in this work can be extended in a straightforward fashion to examine conditions of macroscopic cleavage crack initiation. Provided single-parameter dominance of near-tip fields exists in the flawed structure, results from this study could be used to examine the appropriateness of applying plane strain fracture toughness to the evaluation of circumferential flaws, in particular to those in ring-forged vessels which have no longitudinal welds. In addition, results from this study could also be applied toward the analysis of the effects of thermal streaming on the fracture resistance of circumferentially oriented flaws in a pressure vessel.

KEY WORDS: crack-initiation toughness, generalized plane strain , fracture toughness, micromechanics, slip-line, reactor pressure vessel, ring-forged, thermal streaming, circumferential flaw

Background

For U.S. pressurized-water reactor (PWRs), use of plane strain fracture toughness data to evaluate the potential for initiation of longitudinal flaws in the reactor pressure vessel (RPV) is appropriate when the RPV is subject to loading situations in which the total axial strain is close to zero. However, the above approach may not be appropriate for circumferential flaws. In the case of a circumferential crack the strain parallel to the crack front produced by the pressure-induced hoop stress is positive (Fig. 1). It is well-known from small-specimen testing that loss of plane strain constraint results in ligament contraction along the crack front and an associated increase in resistance to crack initiation [1,2]. For some structural materials, the elevated toughness can be on the order of two to five times the plane strain value. Because a negative strain parallel to the crack front has been demonstrated to be associated with a greater resistance to crack initiation, it is reasonable to suppose that a positive strain parallel to the crack front may be associated with an enhanced tendency toward crack initiation. The point to be made is *not* that transverse strain is necessarily a *cause* of toughness deviation from a reference plane strain value. Rather, available experimental data suggest the possibility of correlating the magnitude of the crack-initiation toughness with the magnitude of the transverse strain. Issues thus arise relative to the application of plane strain fracture toughness to the evaluation of circumferential flaws, particularly to those in ring-forged vessels that have no longitudinal welds [3]. The need for early resolution of these issues is accentuated by the fact that four out of five reactor vessels that currently violate the minimum Charpy upper-shelf requirement given in [4] are of ring-forged construction [5].

Current fracture analysis methods do not provide a straightforward procedure to estimate the effects of positive out-of-plane straining on crack-initiation toughness by extrapolating existing plane stress to plane strain crack-initiation data. Current capability to estimate crack-initiation toughness under conditions of minor relaxation from plane strain is empirical, and methods such as Irwin's β_{Ic} approach [6,7] are physically plausible only for limited deviations from plane strain toward plane stress conditions. Without a better understanding of the correlation between

a critical value of K or J at crack initiation and the associated through-thickness straining conditions in the vicinity of a crack front, it is difficult to justify the use of an extrapolation scheme to estimate effects of positive out-of-plane straining on crack initiation.

Objective and Scope

The objective of this paper is to describe the development of a method for estimating the decrease in crack-initiation toughness, from a reference plane strain value, due to positive straining along the crack front of a circumferential flaw in a reactor pressure vessel (RPV). This paper will present the first phase of this work, which focuses on the development of a slip-line description of the near-tip region based on a generalized plane strain version of the Rice-Johnson model of a blunting crack under plane strain conditions. In addition, the scope of the investigation is limited to crack front constraint conditions that can be described in terms of the conventional one-parameter in-plane K-fields and the transverse strain. Preliminary estimates on the change in crack-initiation toughness associated with either negative or positive straining along a crack front will be presented. It is anticipated that results from the slip-line analysis will be used to guide the development of a finite element description of the near-tip region in the next phase of this study, at which time the effects of the higher order T-stress on crack initiation under generalized plane strain conditions will also be examined.

While this study is intended to address concerns regarding the effects of positive out-of-plane straining on ductile crack initiation, the approach adopted in this work can be extended in a straightforward fashion to examine conditions of macroscopic cleavage crack initiation. Provided single-parameter dominance of near-tip fields exists in the flawed structure, results from this study could be used to examine the appropriateness of applying plane strain fracture toughness to the evaluation of circumferential flaws, in particular to those in ring-forged vessels which have no longitudinal welds. In addition, results from this study could also be applied toward the analysis of the effects of thermal streaming on the fracture resistance of circumferentially oriented flaws in a pressure vessel [8-10].

Micromechanical Approach To Crack-Initiation Prediction

The crack-initiation prediction adopted in this study relates crack initiation under generalized plane strain conditions with material failure at points in the vicinity of a crack front and involves the formulation of a micromechanical crack-initiation model. A micromechanical or near-tip approach to crack-initiation prediction involves not only a proper description of the near-tip stresses and strains at the onset of crack initiation but also considers the microscopic mechanisms through which a macroscopically sharp crack initiates from its original position. While a comprehensive understanding of these aspects of crack initiation is not yet available, *qualitative understandings* of crack initiation have been available for some time. Examples of crack-initiation models using a micromechanical approach can be found in the literature [11-19]. In principle, the micromechanical approach can be validated using plane strain to plane stress crack-initiation data so reasonable confidence in its validity can be established.

The starting point of the micromechanical crack-initiation model involves a description of the stress and strain distributions within a distance of two to three crack-tip-opening displacements (δ_t) directly ahead of a two-dimensional crack front. The essential difference between this formulation and traditional small geometry change (SGC) linear-elastic and elastic-plastic fracture mechanics formulations [20–22] is that large geometry change (LGC) effects in the vicinity of the crack tip are considered. Consideration of LGC effects means that the traditional mathematically sharp crack is now replaced with a blunted notch under load, which is the physically more meaningful crack-tip representation when one is interested in events within a distance of a few δ_t from the deforming crack tip.

The near-tip model of a blunted notch employed in this study is a modified version of the Rice-Johnson (RJ) model of a blunted notch under plane strain conditions [12,23,24]. The modified RJ model presented here is formulated to analyze a blunted notch under generalized plane strain conditions and is identical to the RJ model under plane strain conditions. Both the RJ and the modified RJ models investigate LGC effects by examining the near-tip stress and strain fields using slip-line theory. Use of slip-line theory is properly limited to a rigid, perfectly

(6)

plastic material. However, methodologies exist within the context of both the RJ and the modified RJ models to take into account elastic-plastic and strain-hardening material response in an approximate fashion. Note that the near-tip analysis could be carried out using a finite element description of the near-tip region, and such a description is planned for the next phase of this work. The simplicity and "analytic" nature of the slip-line near-tip formulation, as opposed to the "numerical" nature of a finite element description make the slip-line formulation well suited to revealing qualitatively the effects of generalized plane strain on crack initiation. Essential features of the problem can be readily highlighted and trends in results established. For the purpose of providing preliminary estimates of the effects of transverse straining on fracture toughness, the present methodology is deemed to be adequate for the first phase of this work. Nevertheless, the probable limitations of one-parameter approaches are recognized.

Generalized Plane Strain Rice-Johnson Model

The modified or generalized plane strain RJ model follows closely the development of the RJ model. However, instead of using plane strain slip-line theory, a generalized plane strain description of the slip-lines has been employed. A general derivation of the slip-line equations, for arbitrary values of the uniform out-of-plane strain component ε_z, is a formidable task. Fortunately, in considering the effects of positive out-of-plane straining on crack initiation of circumferential flaws in RPVs, one is interested in values of ε_z that are usually less than, and at most on the order of a few times, the yield strain . Within a region of dimensions comparable in magnitude to a few δ_t ahead of a blunted notch and over the range of values of ε_z of interest in this study, it is anticipated that the out-of-plane stress component σ_z, analogous to its plane strain counterpart, will remain the intermediate principal stress component . This is because, near the crack tip, the value of ε_z is small compared to ε_x and ε_y. Development of the governing equations for generalized plane strain slip-line theory, subject to the stipulation that σ_z remains the intermediate principal stress component, is much more tractable and is presented in [25]. While the generalized plane strain equations given in [25] reduce to their plane strain

counterparts when $\varepsilon_z = 0$, they cannot be used to analyze plane stress problems where $\sigma_z = 0$ for reasons already stated. Associated with the class of generalized plane strain problems examined in [25] are limitations on the forms of the generalized plane strain equations, and these limitations have been made explicit in [25]. Let the degree of out-of-plane straining at a material point be characterized by the value of the function ζ, which takes the form

$$\zeta = \sqrt{1 - \left(\frac{\varepsilon_z}{\varepsilon_e}\right)^2} . \tag{1}$$

In Eq. (1), ε_e is the Mises effective plastic strain defined by the relation

$$\varepsilon_e = \sqrt{\frac{2}{3}\varepsilon_{ij}\varepsilon_{ij}} , \tag{2}$$

where ε_{ij} is the strain tensor. The stipulation that σ_z remains the intermediate principal stress imposes limitations on the allowable range of values for $\varepsilon_z/\varepsilon_e$. Specifically, $\varepsilon_z/\varepsilon_e$ must obey the inequality

$$\left|\frac{\varepsilon_z}{\varepsilon_e}\right| < \frac{1}{2} , \tag{3}$$

such that the function ζ assumes values in the range

$$1 \geq \zeta \geq \frac{\sqrt{3}}{2} . \tag{4}$$

A state of plane strain exists when the function ζ takes on the value of unity. The generalized plane strain, slip-line relations appropriate to both the sharp crack and the blunted notch problems are developed in [25] and summarized in the following sections.

Small Geometry Change Solution

Under generalized plane strain conditions, the plane strain Prandtl stress field indicated in Fig. 2(*a*) is modified as follows. Within regions A and B, the slip-lines gradually deviate from the indicated 45° and 135° inclination with respect to the crack plane as one moves away from the plane of symmetry. This deviation is dependent on the degree of out-of-plane straining ζ. This deviation from "straightness" also applies to the radial slip-lines within the centered fan C. However, the asymptotic nature of the present problem (that is, the small size of the crack tip zone being analyzed as compared to δ_t) permits one to regard the sharp-crack slip-lines as "straight".

Following [12], a deformation theory of plasticity is used to describe the strains, so that the path independent J-integral [23] can be used to obtain simple relations between J, R_{max}, and δ_t. Specifically, these relations subject to plane strain, small-scale-yielding conditions are given in [12] and take the form

$$R_{max} = \frac{3(1-\nu)}{4\sqrt{2}(2+\pi)}\left(\frac{K}{\tau_0}\right)^2 = 0.217\left(\frac{K}{\sigma_0}\right)^2, \tag{5a}$$

$$\delta_t = \frac{2(1-\nu^2)}{2+\pi}\frac{K^2}{E\tau_0} = 0.613\frac{K^2}{E\sigma_0} = 2.8\frac{\sigma_0}{E}R_{max} \tag{5b}$$

where τ_0 is the yield stress in shear. The quantity R_{max} may be regarded as a very approximate measure of the maximum distance to the elastic-plastic boundary along a radial line within the fan. In Eqs. (5a and b) Poisson's ratio is taken to be $\nu = 0.3$. In addition, the Mises shear-tension yield relation is used such that $\sigma_0 = \tau_0\sqrt{3}$, where σ_0 is the yield stress in tension. The coefficients in Eqs. (5a and b) are probably slightly large, and discussions concerning more refined estimates can be found in [12, 16, 26–29]. For the purpose of this study Eqs. (5a and b) are entirely adequate because it is the functional form of these relationships that is of interest.

An important approximation in the RJ model concerns the manner in which the sharp crack, SGC solution provides the appropriate boundary conditions for evaluating the near-tip fields of the blunted notch, LGC problem. From slip-line theory, it is known that straight slip-lines transmit a uniform velocity parallel to themselves. From Eq. (5b), it is seen that δ_t is of the order σ_0/E times the maximum extent R_{max} of the plastic zone. Therefore, region D in Fig. 2(*b*) is typically 2 orders of magnitude smaller than R_{max}, such that when viewed on the larger size scale of the plastic zone in Fig. 2(*a*) region D still appears as a point. It is therefore argued in [12] that the velocities on the boundary of region D are known in terms of velocities in the fan far away from the boundary, and these velocities are then assumed to be given by the velocities in the centered fan of the SGC solution.

The crack-tip-opening displacement, when viewed on the scale of Fig. 2(*b*), is the relevant measure of loading that determines the stress and strain distributions within region D. Conceptually, this is equivalent to taking δ_t as a measure of "time," so the velocities mentioned in the previous paragraph are defined as the rate of change of displacement quantities with δ_t. From [12] the radial velocity v_r within the centered-fan region takes the form

$$V_r(\theta) = \frac{1}{2\sqrt{2}}\left[\cos\left(\theta - \frac{\pi}{4}\right) - \cos\left(2\theta - \frac{\pi}{2}\right)\right] . \qquad (6)$$

Large Geometry Change Solution

Introduce a set of characteristic α,β coordinates into region D as indicated in Fig. 3 (taken from [12]), where lines of β = constant and α = constant are the first and second principal shear directions, respectively. The coordinate origin is located at the apex of region D and is defined such that $\alpha = 0$ and $\beta = \phi - \pi/4$ on the upper boundary of region D and $\beta = 0$ and $\alpha = \phi - \pi/4$ on the lower boundary. The first principal shear angle is denoted as ϕ. The scaling arguments presented in the last section imply that the constant displacement rate V_α, along each straight α line of the LGC noncentered fan, can be approximated by the radial displacement rate V_r of the SGC centered fan, with the shear angle ϕ of the noncentered α lines replacing the polar

coordinate θ (which coincides with the shear angle) for the radial or α lines of the centered fan. Consequently, the velocity normal to the boundary of region D, v_α, now takes the form [12]

$$V_\alpha(\phi) = \frac{1}{2\sqrt{2}} \left[\cos\left(\phi - \frac{\pi}{4}\right) - \cos\left(2\phi - \frac{\pi}{2}\right) \right]. \tag{7}$$

Evaluation of the stress and strain distributions within region D is thus formulated in terms of a boundary value problem with the velocities as unknowns.

The present generalized plane strain study also assumes the validity of a single-parameter description of the near-tip stress and strain fields. Consequently, relations of the type shown in Eqs. (5a and b) also hold in the present case. However, it is not known if the numerical coefficients under generalized plane strain are the same as those in Eqs. (5a and b). For the purpose of comparing crack-initiation toughness values under varying degrees of out-of-plane straining, the plane strain relation Eq. (5b) is assumed to hold under generalized plane strain conditions. Finite element results in [25] indicate that generalized plane strain loading introduces modifications to the plane strain velocity fields [Eq. (6)] within the centered fan. A rigorous finite element treatment of the present problem, for an elastic-plastic material, would entail a Poisson's effect correction of the "remote" boundary conditions in Eq. (7), and the effects of this correction were examined for the SGC problem in [30]. However, it is unclear how this correction could be incorporated into the present slip-line model. In addition, the stipulation of remote elastic K-fields in Eqs. (5a and b) properly limits the allowable range of the out-of-plane strain to less than the yield strain. Within the framework of a slip-line approach and the intent of this study, it is necessary to consider values of the out-of-plane strain that are on the order of a few times the yield strain. As discussed in [25], the perturbations to Eq. (7) due to non-zero values of ε_z are accounted for in this study using an empirical relation. The velocity normal to the boundary of region D, V_α, under generalized plane strain conditions now takes the form

$$\hat{V}_\alpha(\phi)=\frac{(1-2\varepsilon_z)}{2\sqrt{2}}\left[\cos\left(\phi-\frac{\pi}{4}\right)-\cos\left(2\theta-\frac{\pi}{2}\right)\right]. \tag{9}$$

The in-plane velocities within region D, along the characteristic directions, are determined by the solutions to the equations

$$\frac{\partial V_\alpha}{\partial\alpha}+V_\beta=-\frac{\dot{\varepsilon}_z}{2}\frac{\partial S_\alpha}{\partial\alpha}, \tag{10a}$$

and

$$\frac{\partial V_\beta}{\partial\beta}+V_\alpha=-\frac{\dot{\varepsilon}_z}{2}\frac{\partial S_\beta}{\partial\beta}, \tag{10b}$$

where $\dot{\varepsilon}_z$ is the uniform "strain rate" along the out-of-plane direction, and S_α and S_β are dimensional distances along the characteristic coordinate directions. Because δ_t serves as a measure of "time" in this problem, the uniform strain rate $\dot{\varepsilon}_z$ is defined according to the relation

$$\dot{\varepsilon}_z=\frac{d\varepsilon_z}{d\delta_t}=\frac{\varepsilon_z}{\delta_t}. \tag{11}$$

An interpretation of Eq. (11) is that the magnitude of the out-of-plane strain component ε_z is reached when the crack-tip-opening displacement attains the reference steady state value δ_t, such that the generalized plane strain loading situations examined in this study can be considered proportional in nature. Therefore, the quantity ε_z/δ_t in Eq. (11) should be regarded as "constant" during an analysis. Because the derivatives $\partial S_\alpha/\partial\alpha$ and $\partial S_\beta/\partial\beta$ in Eqs.(10a and b) are unknowns themselves, Eqs.(10a and b) need to be evaluated in an iterative manner for the unknown velocities within region D. For the range of ε_z values considered in this study, an efficient iterative scheme is found by using the logarithmic spiral solution associated with a semicircular notch profile as an initial guess for evaluating the derivatives $\partial S_\alpha/\partial\alpha$ and $\partial S_\beta/\partial\beta$. In all cases

considered, less than ten iterations of Eqs.(10a and b) were required to achieve a convergent solution.

Strain Distribution Directly Ahead Of A Blunted Notch

Following [12], solution for the strain distribution directly ahead of the blunted notch tip begins by associating all quantities along the x axis, directly ahead of the notch tip, parametrically in terms of the tangent angle ψ of the point on the notch tip intersected by the β slip-line drawn from the point of interest on the x axis, as schematically shown in Fig. 4. Hence, $\psi = \pi/2$ represents the point on the x axis at the outer extremity or apex of region D. The point at the deformed notch tip on the x axis corresponds to $\psi = 0$. From the velocity solution, the dimensionless x-direction velocity component directly ahead of the blunted notch V_x is known and can be expressed via ψ in the form

$$V_x(x,y)\big|_{y=0} = V(\psi) \, . \tag{12}$$

Let the deformed x-coordinate of a material point corresponding to angle ψ be written in terms of the nondimensional function $F(\psi)$ defined by the relation

$$x = \delta_t \, F(\psi) \, . \tag{13}$$

In the RJ model the distortions occurring ahead of region D, in the neighborhood of the apex, are considered small. As a result, the y-direction or "opening" strain ε_y^{tr} ahead of the blunted notch takes the form

$$\varepsilon_y(\psi) = -\int_{\psi}^{\pi/2} \frac{V'(\eta)}{F(\eta) - V(\eta)} \, d\eta \, . \tag{14}$$

A significant difference between the plane strain RJ model and the modified RJ model used in this study arises from the assumption concerning the state of strain at the apex. The

magnitudes of the strains in the constant stress regions A and B in Fig. 2(*a*) are on the order of the yield strain, and hence the state of strain at the apex in Fig. 3 can be expected to be of similar magnitude. Let $\varepsilon_{\alpha\beta}$ denote the shear strain components along the characteristic directions ahead of the blunted notch. In the plane strain RJ formulation, $\varepsilon_{\alpha\beta} = \varepsilon_y$ along the crack plane, so that use of Eq. (14) within region D implies zero strain at the apex. Evidently, this assumption was deemed acceptable in view of the large strain that develops adjacent to the blunted notch tip. However, it is clear from Eq. (3) that the state of strain must have nonzero values of the in-plane strain components for a state of generalized plane strain to exist at the apex (and throughout the region D). Therefore, inclusion of the small, but nonzero, state of strain at the apex is crucial toward a proper consideration of generalized plane strain effects. For the purpose of comparing the difference in initiation toughness due to non-zero values of the out-of-plane strain ε_z, the assumption is made that a nonzero value of $\varepsilon_{\alpha\beta} = \varepsilon_a$ exists at the apex and that the magnitude of this shear-strain component at the apex is independent of the magnitude of ε_z. The condition governing $\varepsilon_{\alpha\beta}$ at the apex employed in this study is admittedly arbitrary. However, within the context of both the RJ and the modified RJ models, the state of strain at the apex is not quantitatively defined.

Associated with the assumption of $\varepsilon_{\alpha\beta} = \varepsilon_a$ at the apex, Eq. (3) provides the "reality condition" governing the admissible values of ε_z as a function of the assumed state of strain at the apex of the form

$$\left|\frac{\varepsilon_z}{\varepsilon_a}\right| < \frac{2}{3} \,. \tag{15}$$

The y-direction strain at the apex ε_{ya} is related to ε_a via the relation

$$\varepsilon_{ya} = \varepsilon_a - \frac{\varepsilon_z}{2} \,. \tag{16}$$

The x-direction strain at the apex ε_{xa} can then be found via the condition of plastic strain incompressibility. The y-direction strain directly ahead of the blunted notch takes the form

$$\varepsilon_y(\psi) = \varepsilon_{ya} - \int_{\psi}^{\pi/2} \frac{V'(\eta)}{F(\eta) - V(\eta)}\, d\eta \,. \qquad (17)$$

By formally setting the apex shear strain $\varepsilon_a = 0$, the modified RJ relation Eq. (17) can be reduced to its plane strain RJ counterpart Eq. (14).

In presenting numerical results, both the magnitude of the out-of-plane strain ε_z and the apex shear strain ε_a are normalized with respect to the uniaxial yield strain ε_0. The strain distribution normal to the crack plane within region D of Fig. 3 is shown in Figs. 5(*a* and *b*) as a function of the normalized undeformed distance X/δ_t for $\varepsilon_a/\varepsilon_0 = 4$ and three values of $\varepsilon_z/\varepsilon_0$ =- 2, 0, 2. Figures 5 (*a* and *b*) represent the same strain distribution drawn to two different strain scale for clarity. First demonstrated by the plane strain RJ model [12], large strains are predicted directly ahead of the blunted notch when LGC effects near the blunted notch tip are considered in a consistent near-tip formulation. However, these large strains exist only within a distance of less than three δ_t from the blunted tip. A consequence of the limited extent of the large strain region is that in situations where crack initiation involves ductile mechanisms requiring large strains, the opening displacement at initiation must be such that the region D incorporates characteristic microstructural dimensions relevant to the fracture process [12]. Note that a strain singularity is predicted as X approaches zero in the present analysis due to the assumption of a smoothly blunted notch. Plane strain finite element calculations based on a blunted notch profile (Fig. 2*c*) that has included vertices suggest that the magnitude of the opening strain is large but finite as the tip is approached [31]. For the values of $\varepsilon_a/\varepsilon_0$ and $\varepsilon_z/\varepsilon_0$ indicated in Fig. 5, the strain distribution is fairly insensitive to the input parameters except in the immediate neighborhood of the apex.

Stress Distribution Directly Ahead Of A Blunted Notch

Solution for the stress distribution directly ahead of the blunted notch tip in Fig. 3 follows closely the procedures employed in the plane strain RJ model, and therefore only the key steps will be discussed here. Following [12], the uniaxial true stress-strain relation is assumed to take the form

$$\sigma = f\left(\varepsilon^{tr}\right) , \tag{18}$$

where $f(\varepsilon^{tr})$ is the uniaxial hardening relation. The equation for the y-direction "opening" stress directly ahead of the blunted notch, within the intense strain region D in Fig. 2(*b*), then takes the form

$$\sigma_y = \frac{2}{\sqrt{3}} M(\psi) f\left(\frac{2}{\sqrt{3}}\varepsilon_p\right) + \frac{2}{\sqrt{3}} \int_0^{\psi} M(\eta)\, f\left(\frac{2}{\sqrt{3}}\varepsilon_p\right) d\eta \ . \tag{19}$$

where

$$M(\psi) = 1 - \frac{1}{3}\left(\frac{\varepsilon_z}{\varepsilon_e}\right)^2 , \tag{20a}$$

$$\varepsilon_p(\psi) = \sqrt{\varepsilon_y^2 + \varepsilon_z^2 + \varepsilon_y \varepsilon_z} \ , \tag{20b}$$

and ε_y is given by Eq. (17). Under plane strain conditions such that $\varepsilon_z = 0$, $M(\psi) = 1$, and $\varepsilon_p(\psi) = \varepsilon_y$ and the corresponding RJ expression is recovered. Numerical evaluation of Eq. (20) is based on a uniaxial power-law stress-strain relation of the form

$$\frac{\sigma}{\sigma_0} = \left(\frac{\varepsilon^{tr}}{\varepsilon_0}\right)^N = \left(\frac{E\varepsilon^{tr}}{\sigma_0}\right)^N , \tag{21}$$

In Fig. 6 the effect of the magnitude of the apex shear strain on the opening-stress distribution is indicated for input parameter values $N = 0.2$, $\sigma_0/E = \varepsilon_0 = 0.0025$, $\varepsilon_z/\varepsilon_0 = 0$, and

five values of the apex shear strain $\varepsilon_a/\varepsilon_0 = 0$, 1, 2, 3, and 4. The RJ prediction [12] assumes $\varepsilon_{\alpha\beta} = 0$ within region D (Fig. 3) and corresponds to the case $\varepsilon_a/\varepsilon_0 = 0$. Detailed finite-element near-crack-tip results obtained by assuming K-dominated far-field conditions [16] and from various compact-tension specimen geometries [32] indicate that the apex shear strain ε_a is on the order of a few times the yield strain ε_0. Note that there is actually a stress singularity predicted in the hardening cases at X = 0, although the singularity is weak and dominates over a very small distance relative to δ_t as shown in Fig. 6. Physically, this upturn in stress as X approaches zero can be disregarded for two reasons: (1) this upturn in stress is a consequence of the continuously hardening stress-strain relation adopted in Eq. (21), and the stress would saturate if a limiting flow stress is imposed on Eq. (21); and (2) the region of dominance of the singular stress is much less than one δ_t so that its physical relevance can be questioned. Disregarding the stress singularity, it is seen that a stress maximum is predicted at a finite distance ahead of the blunted notch tip when LGC effects are considered, in contrast to SGC, sharp crack analyses. This stress maximum occurs either within the large-strain region, or at the location where the large-strain stress solution intersects the small-strain solution. Note that both the value and the location of the stress maximum are strongly dependent on the assumed apex strain state. The concept of a maximum achievable stress suggests the possibility of abrupt toughness transitions with temperature or loading rate in materials susceptible to stress-controlled cleavage failure [12]. This observation has important consequences with regard to the application of conventional cleavage failure models, which consider cleavage failure to be possible when the maximum achievable stress exceeds a material failure stress over a microscopically significant distance, generally on the order of a few grain diameters.

In Fig. 7 the effect of out-of-plane straining on the opening stress distribution is indicated for input parameter values N = 0.2, $\sigma_0/E = 0.0025$, $\varepsilon_a/\varepsilon_0 = 4$, and three values of the out-of-plane strain $\varepsilon_z/\varepsilon_0 = -2$, 0, and 2. It is seen that deviation from plane strain constraint results in either minimal change or a decrease in the value of the opening stress ahead of the blunted notch. While a decrease in σ_y under less than plane strain conditions appears consistent with observed

cleavage toughness trends, the rather pronounced reduction in σ_y due to positive out-of-plane straining is counter-intuitive. Discussions on the observed trends for σ_y can be found in [25]. Implications of the present results regarding (ductile) toughness predictions under generalized plane strain conditions are presented in the next section.

Material Failure Criteria and Crack-Initiation Toughness Prediction

A number of material failure criteria exist in the literature, all of which seek to correlate the attainment of a critical value of the macroscopic fracture parameter, such as K or J, with more fundamental material properties such as limiting stresses and strains. Because fracture parameters involve a length dimension, an empirical microscopic length parameter—such as mean grain size or mean void spacing—is usually associated with these material failure criteria. In situations where the material failure process is ductile in nature, it is commonly accepted that the failure strains are sensitive to the associated stress state.

A simple ductile failure criterion is adopted in this study to estimate the decrease in crack-initiation toughness, from a reference plane strain value, due to positive straining along the crack front. This material failure criterion assumes that crack initiation can be expressed in terms of critical values of global or macroscopic stress and strain parameters and is similar to the simpler of the two failure criteria used in [12]. Specifically, the Mises effective strain directly ahead of the blunted notch is assumed to be the limiting strain parameter, and the critical value of this strain parameter at failure is assumed to be a function of the associated triaxial stress state at the material point. Following [14,15], the material failure criterion is assumed to take the simple form

$$\varepsilon_e^f = \alpha\, e^{\left(-\frac{3}{2}\frac{\sigma_m}{\sigma_e}\right)} \quad , \tag{22}$$

where σ_m is the mean stress, ε_e and σ_e are the Mises effective stress and strain, and α is the value of the failure strain as the triaxial stress ratio σ_m/σ_e approaches zero. Motivation for the

functional form of Eq. (22) comes from various theoretical analyses [11,33] which suggest that the growth of voids is strongly dependent on the state of triaxial stress in the vicinity of these voids. In Fig. 8 (taken from [15]), the experimentally determined material failure curves are shown for a wide variety of materials. The failure curves are strong functions of the materials of interest, and thus application of Eq. (22) to toughness prediction requires the generation of a failure curve appropriate to the material under investigation. Two curves corresponding to $\alpha = 1$ and $\alpha = 2$ have been included in Fig. 8 for comparison with other experimentally generated failure curves.

In the first phase of this work, a hypothetical failure curve corresponding to $\alpha = 1$ in Eq. (22) is used to examine the influence of out-of-plane straining on the deviation from plane strain crack-initiation toughness. Note that, in general, the results to be presented based on $\alpha = 1$ will not be quantitatively correct for RPV grade materials such as A533B at a given temperature. The limiting values of ε_e associated with the $\alpha = 1$ curve and various values of ε_z are determined as the intersection of the $\alpha = 1$ curve with the calculated stress-strain distributions. The corresponding critical values of the normalized distance parameter X/δ_t ahead of the blunted notch tip can be related to a critical value of the fracture parameter K or J via relations of the type indicated in Eq. (5b). Prediction of the absolute magnitude of the fracture parameter at initiation ($K = K_c$) requires that a definite value of the characteristic distance variable $X = X_c$ be available. Previous attempts at fracture toughness predictions based on definite values of X_c can be found in [12,14]. In determining the relative change in initiation toughness due to ε_z, it is only necessary to assume X_c is independent of ε_z. With the further assumption that the numerical coefficient in Eq. (5b) is also independent of ε_z, an assumption that appears to be well supported by the finite element results in [25], the relative change in initiation toughness can be determined from the relation

$$\frac{K_c}{K_{Ic}} = \sqrt{\frac{\delta_{Ic}}{\delta_c}} \quad , \tag{23}$$

where (K_c, δ_c) are the critical values of K and δ_t associated with a nonzero value of ε_z, and (K_{Ic}, δ_{Ic}) are the critical values of K and δ_t associated with the plane strain conditions corresponding to $\varepsilon_z = 0$. Toughness predictions based on this procedure are summarized in Table 1 for input parameters $\sigma_0/E = 0.0025$, $\varepsilon_a/\varepsilon_0 = 4$, N = 0, 0.1 and three values of $\varepsilon_z/\varepsilon_0 = -2$, 0, and 2.

Results in Table 1 indicate minimal change in the initiation toughness for the given choice of input parameters. It should be re-emphasized that the material failure curve associated with $\alpha = 1$ is chosen merely to illustrate the manner in which the present analysis method could be used to predict crack-initiation toughness. In addition, the results in Table 1 are strongly dependent on the assumed form of the material failure criterion. The implication of these calculations is that the decrease in crack-initiation toughness from a reference plane strain value due to a moderate degree of out-of-plane straining is minimal, provided the stress and strain states in the vicinity of the crack tip can be characterized by a one-parameter K field. Obviously, this observation must be considered tentative, and much more work remains to validate the assumptions and to improve the approximations used in the present analysis.

Discussion

Limited biaxial studies on part-through, surface-cracked plates [34,35] indicate that the crack-initiation toughness expressed in terms of the stress intensity factor K is rather insensitive to the range of biaxial loading examined in those studies under *cleavage* crack-initiation conditions. However, it is significant that the implications from the present near-tip analysis stand in constrast with wide-plate results presented in [36,37]. As dicussed in [25], it is believed that a two-parameter approach is needed to characterize crack initiation in some of the wide-plate tests. Use of the present approach to predict crack initiation under positive out-of-plane straining conditions for a circumferential flaw awaits the determination of the near-tip stress and strain fields appropriate to pressure vessel applications.

REFERENCES

[1] S. T. Rolfe and J. M. Barsom, *Fracture and Fatigue Control in Structures: Applications of Fracture Mechanics*, Prentice-Hall Inc., Englewood, N.J., 1977.

[2] M. F. Kanninen and C. H. Popelar, *Advanced Fracture Mechanics*, Oxford University Press, New York, 1985.

[3] W. E. Pennell, Martin Marietta Energy Systems, Inc., Oak Ridge Natl. Lab., "Heavy Section Steel Technology Program Fracture Issues," pp. 1–26 in *Proceedings of the USNRC Seventeenth Water Reactor Safety Information Meeting*, USNRC Conference Proceedings NUREG/CP-0105, Vol. 3, March 1990.

[4] *Code of Federal Regulations*, Title 10, Part 50, Section 50.61 and Appendix G.

[5] J. G. Merkle, Martin Marietta Energy Systems, Inc., Oak Ridge Natl. Lab., *An Overview of the Low-Upper-Shelf Toughness Safety Margin Issue*, USNRC Report NUREG/CR-5552 (ORNL/TM-11314), August 1990.

[6] G. R. Irwin, "Fracture Mode Transition for a Crack Traversing a Plate," *Journal of Basic Engineering*. 82(2), 417–25 (1960).

[7] J. G. Merkle, Martin Marietta Energy Systems, Inc., Oak Ridge Natl. Lab., *An Examination of the Size Effects and Data Scatter Observed in Small-Specimen Cleavage Fracture Toughness Testing*, USNRC Report NUREG/CR-3672 (ORNL/TM-9088), August 1984.

[8] T. G. Theofanous and K. Iyer, "Mixing Phenomena of Interest to SBLOCAs," *Nuclear Engineering and Design* 102, 91–103, (1987).

[9] K. Kussmaul et al., "Cyclic and Transient Thermal Loading of the HDR Reactor Pressure Vessel with Respect to Crack Initiation and Crack Propagation," in *Proceedings of the Sixth International Seminar on Assuring Structural Integrity of Steel Reactor Pressure Boundary Components: SMIRT-10 Post Conference Seminar No. 2, 1989.*

[10] M. Kuna, H. Kordisch, and A. Ockewitz, "Thermoelastic-Plastic FEM-Analysis of a Semi-Elliptical Surface Crack in a Cylinder Under Non-Axial-Symmetric Cooling," in *Proceedings of the European Symposium on Elastic-Plastic Fracture Mechanics: Elements of Defect Assessment October 9–12, 1989, Freiburg, FRG*, to be published by Institute of Mechanical Engineers, London, 1991.

[11] F. A. McClintock, "A Criterion for Ductile Fracture by the Growth of Holes," *Journal of Applied Mechanics* 35, 363–371 (1968).

[12] J. R. Rice and M. A. Johnson, "The Role of Large Crack Tip Geometry Changes in Plane Strain Fracture," in *Inelastic Behavior of Solids* (McGraw-Hill, New York, 1977), pp. 641–672.

[13] R. O. Ritchie, J. F. Knott, and J. R. Rice, "On the Relationship Between Critical Tensile Stress and Fracture Toughness in Mild Steel," *Journal of the Mechanics and Physics of Solids* 21, 395 (1973).

[14] J. W. Hancock and A. C. MacKenzie, "On the Mechanisms of Ductile Failure in High-Strength Steels Subjected to Multi-Axial Stress-States," *Journal of the Mechanics and Physics of Solids* 24, 147–169 (1976).

[15] A. C. MacKenzie, J. W. Hancock, and D. K. Brown, "On the Influence of State of Stress on Ductile Failure Initiation in High Strength Steels," *Engineering Fracture Mechanics* 9, 167–188 (1985).

[16] R. M. McMeeking, "Finite Deformation Analysis of Crack-Tip Opening in Elastic-Plastic Materials and Implications for Fracture," *Journal of the Mechanics and Physics of Solids* 25, 357–381 (1977).

[17] N. Aravas and R. M. McMeeking, "Finite-Element Analysis of Void Growth Near a Blunting Crack-Tip," *Journal of the Mechanics and Physics of Solids* 33, 25–49 (1985).

[18] A. Needleman and V. Tvergaard, "An Analysis of Ductile Rupture Modes at a Crack Tip," *Journal of the Mechanics and Physics of Solids* 35, 151–183 (1987).

[19] D. Teirlinck et al., "Fracture Mechanism Maps in Stress Space," *Acta Metallurgica.* 36(5), 1213–1228 (1988).

[20] G. R. Irwin, "Fracture Mechanics," in *Structural Mechanics*, Pergamon Press, 1960, pp. 557–594.

[21] J. W. Hutchinson, "Singular Behavior at the End of a Tensile Crack in a Hardening Material," *Journal of the Mechanics and Physics of Solids* 16, 13–31 (1968).

[22] J. R. Rice and G. F. Rosengren, "Plane Strain Deformation Near a Crack Tip in a Power-Law Hardening Material," *Journal of the Mechanics and Physics of Solids* 16, 1–12 (1968).

[23] J. R. Rice, "A Path Independent Integral and the Approximate Analysis of Strain Concentration by Notches and Cracks," *Journal of Applied Mechanics.* 35, 379–386 (1968).

[24] J. R. Rice, "Mathematical Analysis in the Mechanics of Fracture," in *Fracture: An Advanced Treatise*, H. Liebowitz, Ed. Vol. II, (Academic Press, New York, 1968), pp. 191–311.

[25] D.K.M. Shum et al, Martin Marietta Energy Systems, Inc., Oak Ridge Natl. Lab., *Analytical Studies of Transverse Strain Effects on Fracture Toughness for Circumferentially Oriented Cracks*, USNRC Report NUREG/CR-5592 (ORNL/TM-11581), February 1991.

[26] N. Levy et al., "Small Scale Yielding Near a Crack in Plane Strain: A Finite Element Analysis," *International Journal of Fracture Mechanics* 7(2), 143–156 (June 1971).

[27] J. R. Rice and D. M. Tracey, "Computational Fracture Mechanics," in *Numerical and Computer Methods in Structural Mechanics* (Academic Press, Inc., New York, 1973), pp. 585–623.

2-3

[28] J. R. Rice, "Elastic-Plastic Fracture Mechanics," *The Mechanics of Fracture, AMD* 19, 23–53 (1976).

[29] D. M. Tracey, "Finite Element Solutions for Crack-Tip Behavior in Small-Scale Yielding," *Journal of Engineering Material and Technology,* 146–151 (April 1976).

[30] D.M. Parks and Y.Y. Wang, "Three-Dimensional Crack Front Constraint", paper presented at the Constraint Working Group Meeting, University of Illinois, Champaign-Urbana, Illinois, February 27, 1990.

[31] R. M. McMeeking, "Blunting of a Plane Strain Crack Tip into a Shape with Vertices," *Journal of Engineering Material and Technology,* 99, 290–297 (1977).

[32] D. Aurich and E. Sommer, "The Effect of Constraint on Elastic-Plastic Fracture," *Steel Research* 8, 358–367 (1988).

[33] J. R. Rice and D. M. Tracey, "On the Ductile Enlargement of Voids in Triaxial Stress Fields," *Journal of the Mechanics and Physics of Solids*17, 201–217 (1969).

[34] S. J. Garwood and T. G. Davey, "Behavior of A533B under Biaxial Loading at +70°C," *International Journal of Pressure Vessel and Piping* 36, 199–224 (1989).

[35] S. J. Garwood, T. G. Davey, and Y. C. Wong, "The Effect of Biaxial Loading on A533B in the Ductile/Brittle Transition," paper presented at the 21st National Symposium on Fracture Mechanics, Annapolis, Md., June 28-30, 1988.

[36] D. J. Naus et al., Martin Marietta Energy Systems, Inc., Oak Ridge Natl. Lab., *High-Temperature Crack-Arrest Behavior in 152-mm-Thick SEN Wide Plates of Quenched and Tempered A 533 Grade B Class 1 Steel,* USNRC Report NUREG/CR-5330 (ORNL/TM-11083), April 1989.

(24)

[37] D. J. Naus et al., Martin Marietta Energy Systems, Inc., Oak Ridge Natl. Lab., *High-Temperature Crack-Arrest Tests Using 152-mm-Thick SEN Wide Plates of Low-Upper-Shelf Base Material: Tests WP-2.2 and WP-2.6*, USNRC Report NUREG/CR-5450 (ORNL/TM-11352), February 1990.

(25)

Table 1-- Toughness predictions based on yield strain $\sigma_0/E = 0.0025$ and apex strain $\varepsilon_a/\varepsilon_0 = 4$ as a function of the degree of strain hardening N and the degree of out-of-plane straining $\varepsilon_z/\varepsilon_0$

N	$\varepsilon_z/\varepsilon_0$	ε_e	X/δ_t	K_c/K_{Ic}
	-2	0.108	1.232	1.009
0	0	0.101	1.255	1
	2	0.095	1.280	0.990
	-2	0.059	1.465	1.026
0.1	0	0.049	1.542	1
	2	0.040	1.625	0.974

Figure Captions

FIG. 1--Configuration of circumferential flaw in weld of ring-forged reactor vessel showing positive tensile hoop strains parallel to the crack front.

FIG. 2--(a) Prandtl slip line construction of near crack tip stress state for contained yielding of an ideally plastic material. This slip line field corresponds to singular strains in the fan region, and results in a non-zero value of the crack tip opening displacement; (b) Slip line construction for the blunted notch region assuming a smooth blunted notch tip profile; (c) Slip line construction for the blunted notch region assuming sharp vertices exist along the notch tip.

FIG. 3--Schematic illustrating the definition of the slip line coordinate system (α,β) in the neighborhood of the blunted notch. The first principal shear angle is denoted as ϕ.

FIG. 4--Schematic illustrating the definition of the tangent angle ψ associated with location along the x axis directly ahead of the blunted notch tip. The point at the deformed notch tip on the x axis corresponds to $\psi = 0$.

FIG. 5(*a*)--Distribution of the "opening" strain ε_y normal to the crack plane as a function of normalized undeformed distance X/δ_t. Note that large strains are predicted ahead of the blunted notch; (*b*) Distribution of the "opening" strain ε_y normal to the crack plane redrawn on a different scale along the strain axis. Note that for values of the out-of-plane strain component ε_z up to 2X the yield strain ε_0, the effect on the ε_y strain distribution is minimal.

FIG. 6--Distribution of the "opening" stress σ_y normal to the crack plane as a function of normalized undeformed distance X/δ_t. Disregarding the spurious stress singularity, it is seen that a stress maximum that is strongly dependent on the value of the apex shear strain ε_a is predicted at a finite distance ahead of the blunted notch tip.

FIG. 7--Distribution of the "opening" stress σ_y normal to the crack plane as a function of normalized undeformed distance X/δ_t. Note that deviation from plane strain constraint results in either minimal change or a decrease in the value of σ_y ahead of the blunted notch.

FIG. 8--Material failure curves for a variety of structural materials. It is seen that the shapes of these failure curves are strongly dependent on the material of interest. Material failure curves corresponding to $\alpha = 1$ and $\alpha = 2$ in Eq. (23) are indicated for comparison.

Top

ORNL DWG 80-5080 ETD

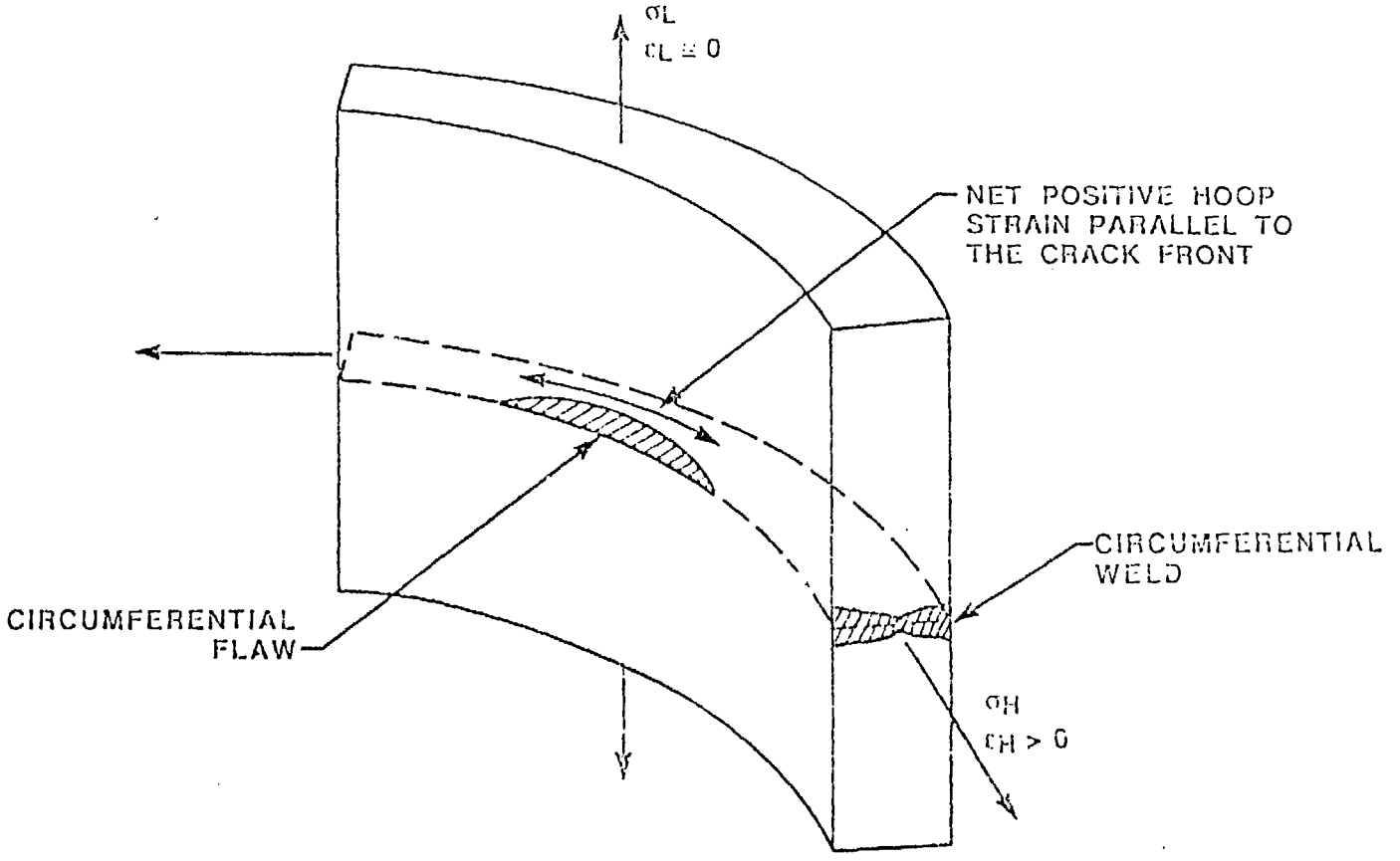

Fig 1

Bottom

Shum + Hoekstra

TOP

CRNL-DWG 90-4183 ETD

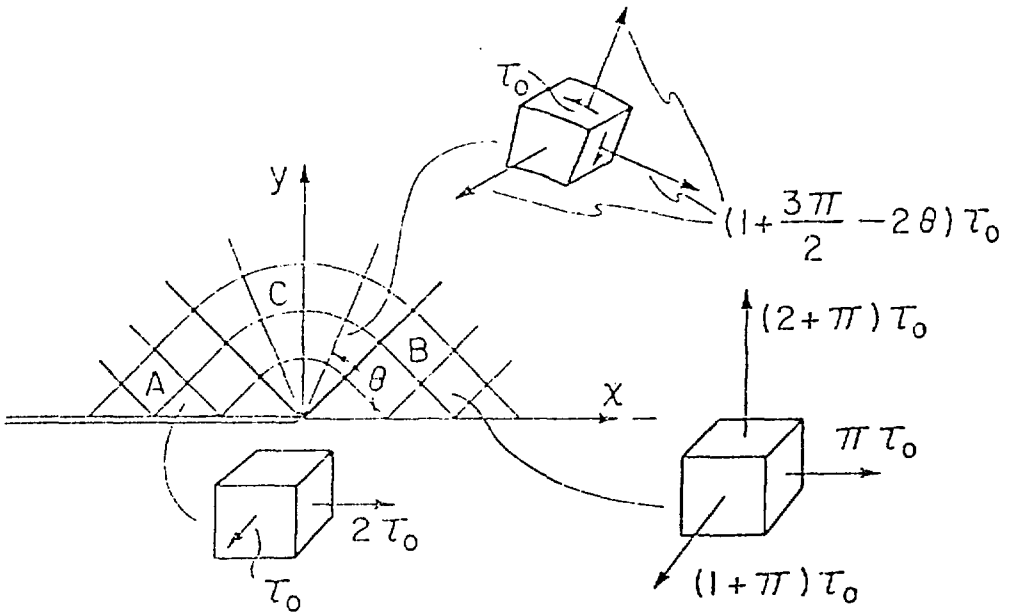

(a)

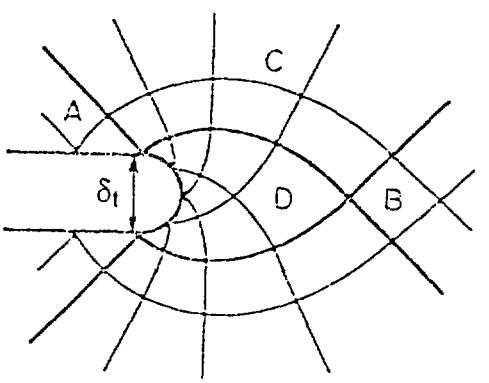

(b)

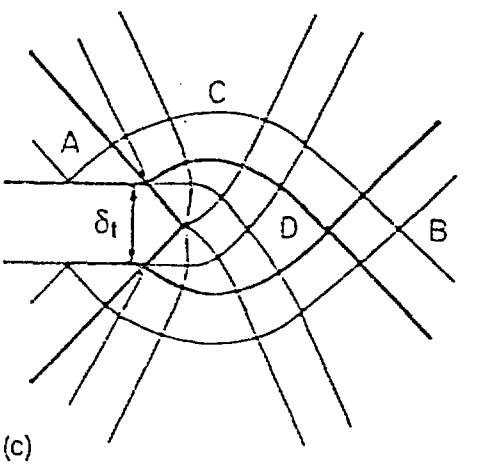

(c)

Fig 2 Shunt Marble BOTTOM

TOP

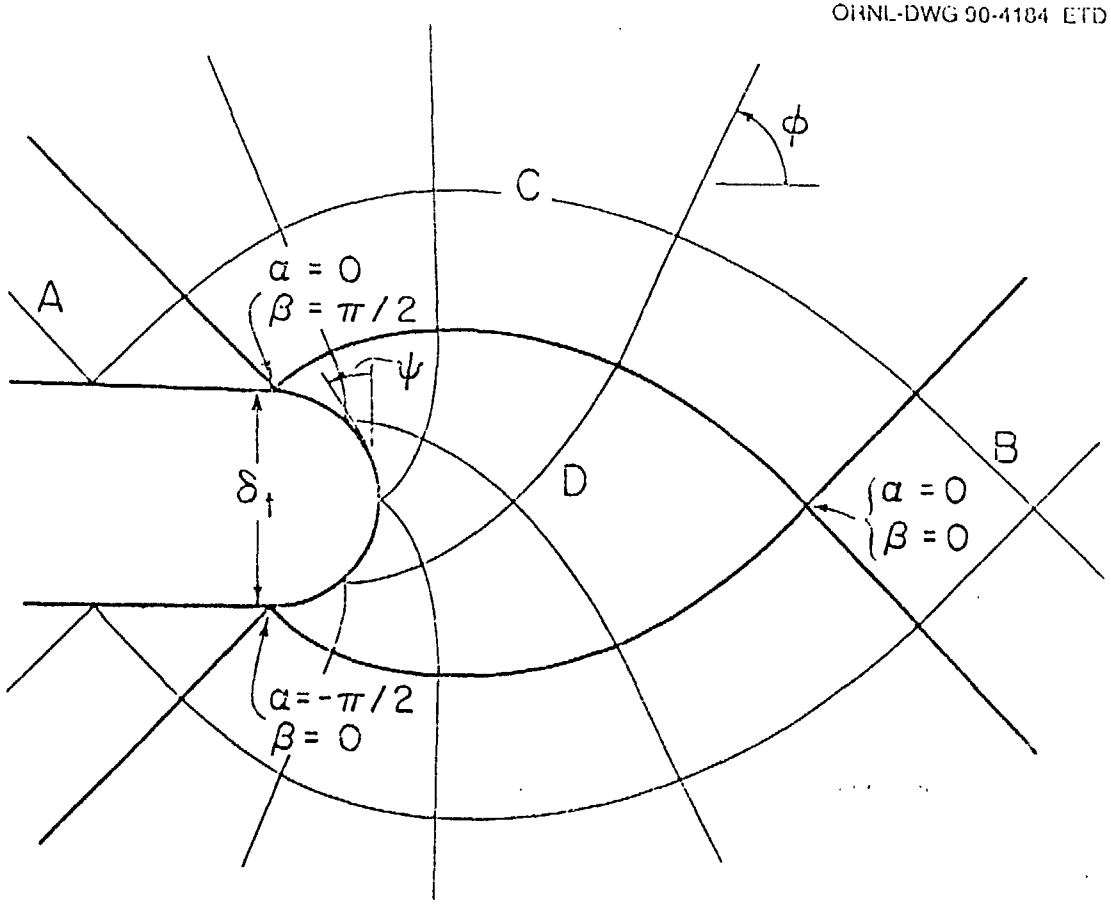

Fig 3 BOTTOM Shaw / Marble

TOP

ORNL-DWG 90M-4185 FED

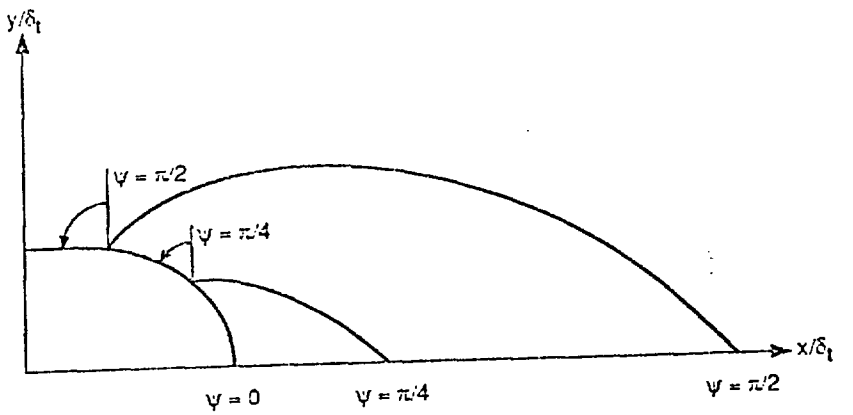

Fig 4

BOTTOM

Shum + Kerrible

TOP

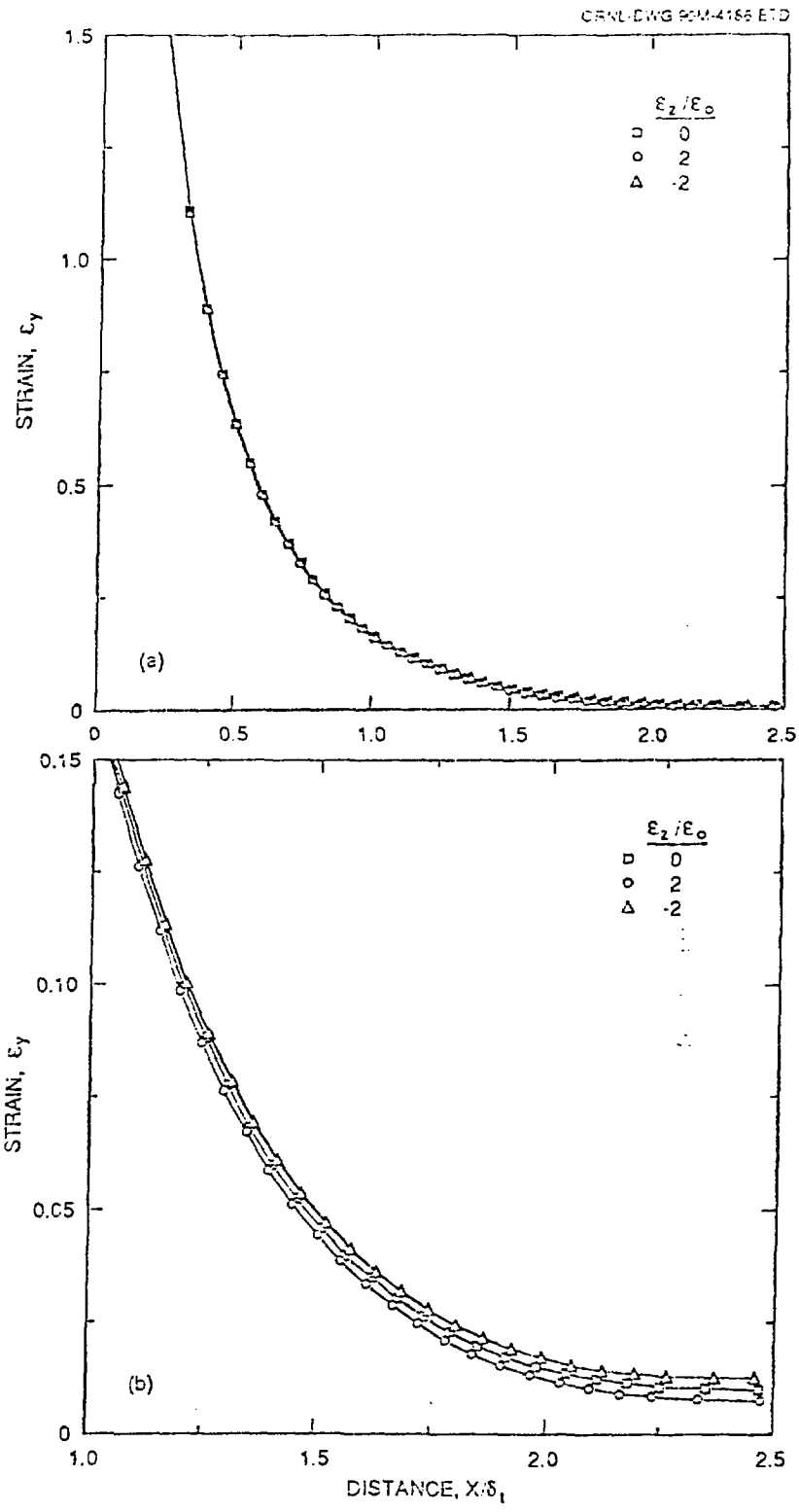

Fig 5a

Fig 5b
Short
Marble

BOTTOM

TOP

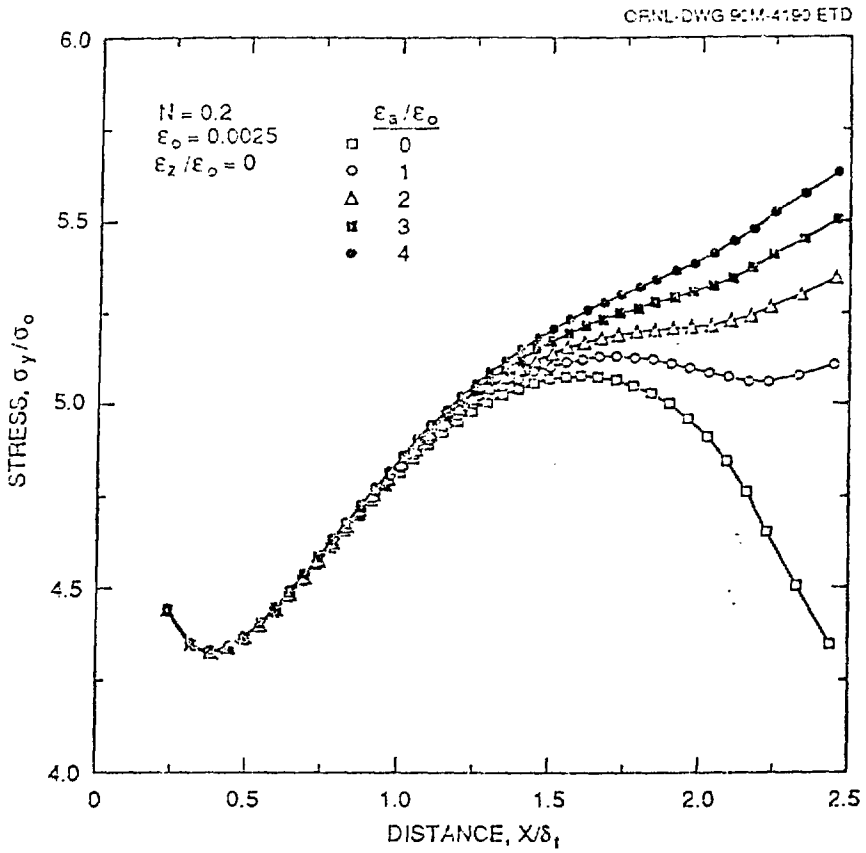

BOTTOM

Fig 6
Shum + Merkle

TOP

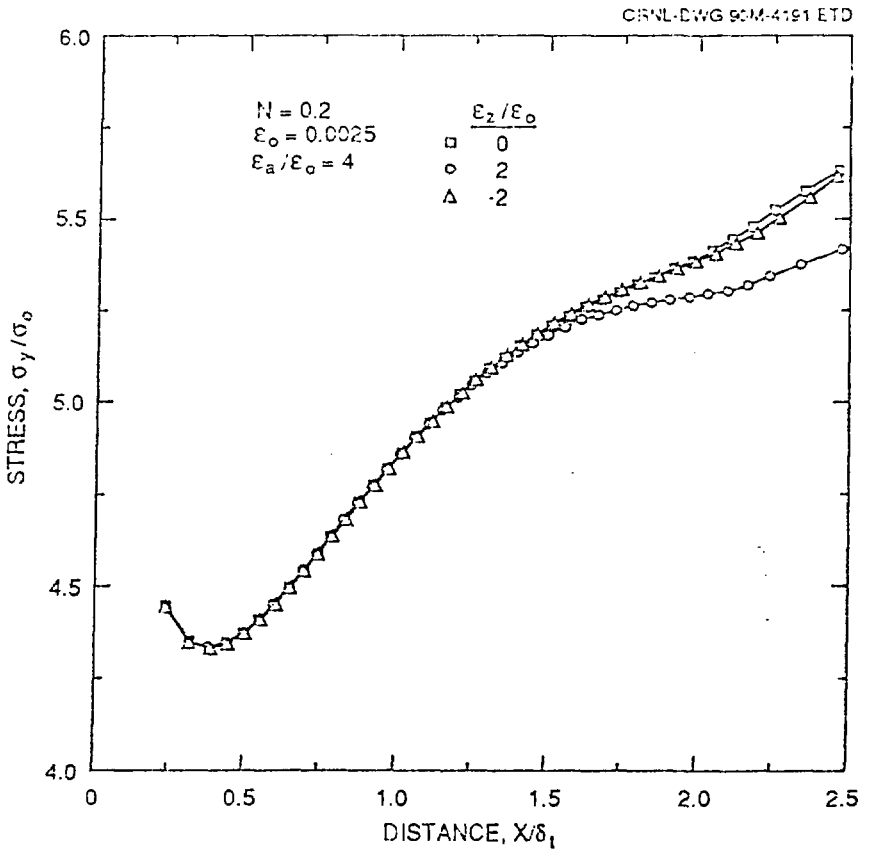

BOTTOM

Fig 7 Shum + Merkle

TOP

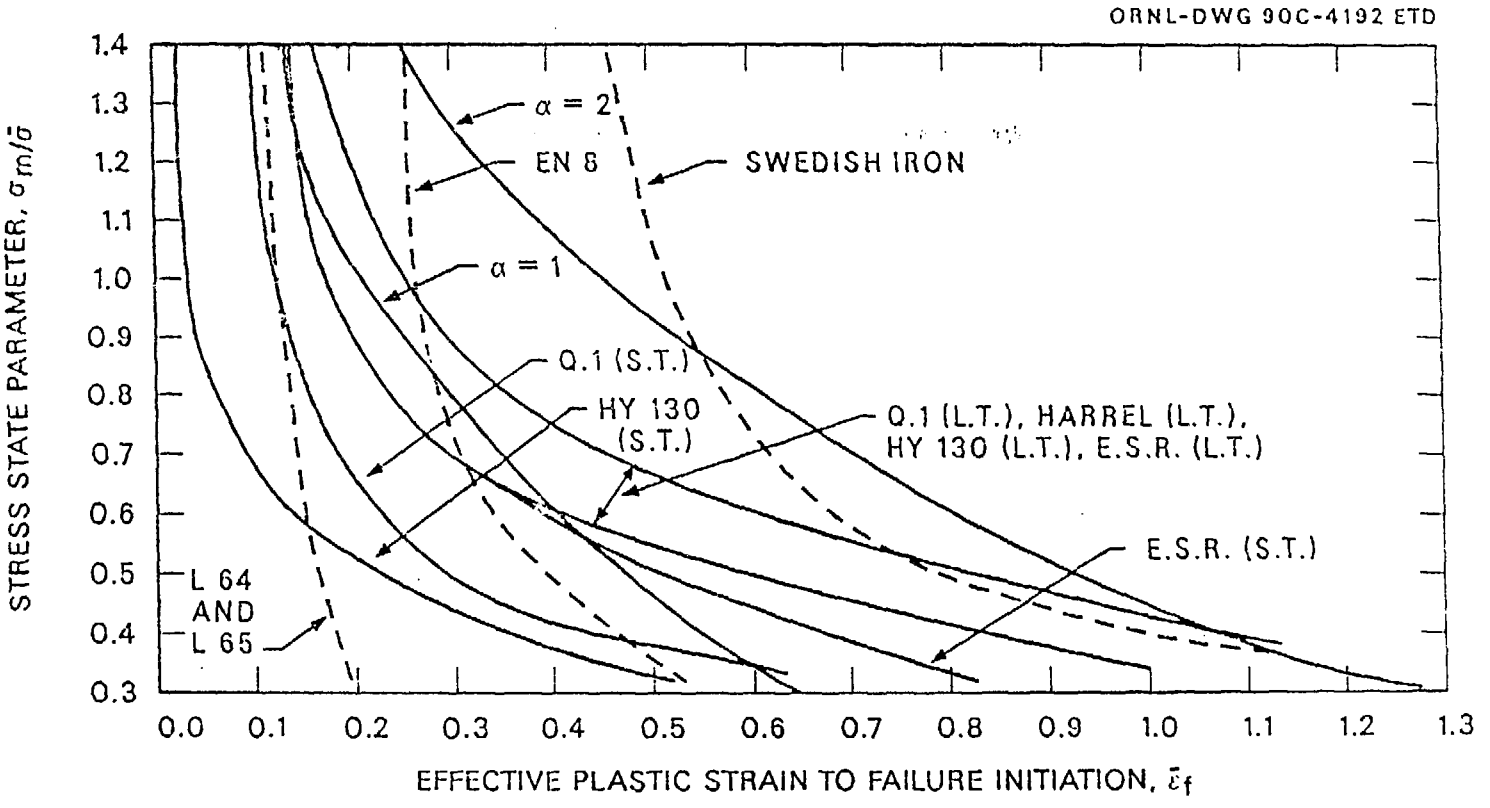

Fig 8 Schumann-Hardtle

BOTTOM